Toxicology and Applied Pharmacology 409 (2020) 115302

Contents lists available at ScienceDirect

Toxicology and Applied Pharmacology

journal homepage: www.elsevier.com/locate/taap

Differential responses of murine alveolar macrophages to elongate mineral particles of asbestiform and non-asbestiform varieties: Cytotoxicity, cytokine secretion and transcriptional changes☆

T.O. Khaliullin [a,b], E.R. Kisin [b], S. Guppi [b], N. Yanamala [a,c], V. Zhernovkov [d], A.A. Shvedova [a,b,*]

[a] West Virginia University, Morgantown, WV, United States of America
[b] HELD, NIOSH, CDC, Morgantown, WV, United States of America
[c] Carnegie Mellon University, Pittsburgh, PA, United States of America
[d] University College Dublin, Dublin, Ireland

ARTICLE INFO

Keywords:
Alveolar macrophage
Elongate mineral particle
Asbestos
Cleavage fragments
RNAseq

ABSTRACT

Human exposures to asbestiform elongate mineral particles (EMP) may lead to diffuse fibrosis, lung cancer, malignant mesothelioma and autoimmune diseases. Cleavage fragments (CF) are chemically identical to asbestiform varieties (or habits) of the parent mineral, but no consensus exists on whether to treat them as asbestos from toxicological and regulatory standpoints. Alveolar macrophages (AM) are the first responders to inhaled particulates, participating in clearance and activating other resident and recruited immunocompetent cells, impacting the long-term outcomes. In this study we address how EMP of asbestiform versus non-asbestiform habit affect AM responses. Max Planck Institute (MPI) cells, a non-transformed mouse line that has an AM phenotype and genotype, were treated with mass-, surface area- (s.a.), and particle number- (p.n.) equivalent concentrations of respirable asbestiform and non-asbestiform riebeckite/tremolite EMP for 24 h. Cytotoxicity, cytokines secretion and transcriptional changes were evaluated. At the equal mass, asbestiform EMP were more cytotoxic, however EMP of both habits induced similar LDH leakage and decrease in viability at s.a. and p.n. equivalent doses. DNA damage assessment and cell cycle analysis revealed differences in the modes of cell death between asbestos and respective CF. There was an increase in chemokines, but not pro-inflammatory cytokines after all EMP treatments. Principal component analysis of the cytokine secretion showed close clustering for the s.a. and p.n. equivalent treatments. There were mineral- and habit-specific patterns of gene expression dysregulation at s.a. equivalent doses. Our study reveals the critical nature of EMP morphometric parameters for exposure assessment and dosing approaches used in toxicity studies.

1. Introduction

The history of prolonged and sometimes uncontrolled exposures in occupational and natural settings has proved that, upon inhalation, airborne elongate mineral particles (EMPs) can cause pulmonary inflammation, fibrosis and cancer (Lippmann, 2014; IARC, 2012; IARC, 2017; Manning et al., 2002), signifying the healthcare and economic burden worldwide. Adverse health outcomes following exposures to asbestos – a commercial term encompassing asbestiform varieties of six different minerals – were studied the most. However, EMP itself is a much broader term, defined as "any mineral particle with a minimum aspect ratio of 3:1" (Middendorf et al., 2011). That includes particles with varied crystal growth habits, such as asbestiform (long, thin, splayed ends) and non-asbestiform (usually short, thick, brittle); the topic is covered in detail by Belluso et al. (Belluso et al., 2017). For more information on the complex asbestos-related terminology, we refer interested readers to appropriate reviews/tabulations (Lowers et al., 2002).

During mining, milling, and processing, non-asbestiform mineral varieties can break down into elongate particles, also known as cleavage fragments (CF). Sometimes that patterned breakage results in dimensions akin to asbestiform fibers. CF might be chemically identical to

☆ A summary sentence: Elongate mineral particles of asbestiform and non-asbestiform varieties induce differential responses in alveolar macrophages

* Corresponding author at: CDC/NIOSH, 1095 Willowdale Road, Morgantown, WV 26505, United States of America.
E-mail addresses: ved2@cdc.gov, tokhaliullin@mix.wvu.edu (T.O. Khaliullin), edk8@cdc.gov (E.R. Kisin), mzi6@cdc.gov (S. Guppi), naveena.yanamala.m@wvumedicine.org (N. Yanamala), vadim.zhernovkov@ucd.ie (V. Zhernovkov), ats1@cdc.gov (A.A. Shvedova).

https://doi.org/10.1016/j.taap.2020.115302
Received 26 September 2020; Received in revised form 17 October 2020; Accepted 21 October 2020
Available online 24 October 2020

asbestiform variety of the same mineral, but there is no consensus between different groups (regulators and scientific communities) on whether to treat them exactly as asbestos in terms of their potential health effects. Inability to reliably predict the occurrence and development of health outcomes after exposure to inhaled EMPs poses a significant challenge to health professionals. The latest professional conference on EMPs has shown that there is still uncertainty, whether some EMPs should be "regulated" (treated similar to asbestos by regulatory agencies) or not (Berman et al., 2018). Of particular concern are the emerging cases of workplace and incidental exposures to EMPs such as those present in vermiculite in Libby, Montana, USA (Dunning et al., 2012; Miller, 2014), erionite in Oregon, USA and Turkey (Dikensoy, 2008), silicon carbide fibers in Norway (Bugge et al., 2012), sodic amphiboles in Nevada and Arizona, USA (Metcalf and Buck, 2015; Pfau et al., 2017), and non-asbestiform EMPs in taconite, talc and gold mining (Mandel et al., 2016).

Epidemiological studies in talc, taconite, and gold mine workers exposed to non-asbestiform EMPs revealed little if any risk of lung cancer or mesothelioma (Allen et al., 2015; Garabrant and Pastula, 2018; Pira et al., 2017), but consistent findings of pneumoconiosis and cardiovascular mortality excess occur in each of these mining types (Mandel et al., 2016; Pira et al., 2017). Limited data exist on the health effects of tremolite and riebeckite CF exposure. There is some epidemiological evidence for tremolite CFs and short (shorter than 10 μm) tremolite asbestos fibers to be the cause of pulmonary fibrosis and lung cancer in nephrite carvers and quarry workers (Yang et al., 2013a; Yang et al., 2013b; Kohyama et al., 2017).

Accumulated data suggests that fiber dose, number, dimensions, durability, surface reactivity, surface area, and their propensity to split into thin fibers in vivo are important mediators of asbestos-related diseases (Lippmann, 1990a; Baron, 2001). Relatively few EMPs with diameters larger than ~3 μm will penetrate into the lungs (Lippmann, 1990b), but those with diameters less than 0.1 μm are also less retained in the lungs compared to larger diameters (Lippmann and Timbrell, 1990). The World Health Organization (WHO) considers EMPs longer than 5 μm "critical" for lung pathology development (World Health, 2000); however, there are propositions to only consider fibers longer than 10 μm (Berman and Crump, 2008; Roggli, 2018) as dangerous for human health. Bearing in mind the inferred importance of fiber dimensions, most of the exposure assessment methods for regulated EMPs are based on "counts". Thus, it is crucial to know exactly what must be counted and what should be "censored" during the counting process. This was brought up in a recent extensive review by Egilman et al. (Egilman et al., 2019).

In 2011 the National Institute for Occupational Safety and Health (NIOSH) published its Current Intelligence Bulletin 62 - Asbestos Fibers and Other Elongate Mineral Particles: State of the Science and Roadmap for Research. In the concluding part, this document has indicated two major research needs that have to be addressed: "…(1) for the asbestos minerals, development of a clearer understanding of the important dimensional and physicochemical determinants of pathogenicity; (2) for other EMPs, such as those from non-asbestiform habits of the asbestos minerals and erionite, development of a deeper understanding of the determinants of toxicity…" (Middendorf et al., 2011). Since then, a number of studies have investigated the role of dimensions and physicochemical properties of asbestos particles (Padmore et al., 2017; Pacella et al., 2012; Duncan et al., 2014; Ishida et al., 2019). There were, however, very limited efforts in elucidating the potential determinants of toxicity of non-asbestiform EMPs, mostly dating back to 1970–90s and the major biological effects found in the studies related not to the number of particles or mass, but to the surface area of the samples (Castranova et al., 1994; Palekar et al., 1979). Studies comparing short and long asbestos fibers were much more prevalent. For instance, short riebeckite asbestos fibers, fully phagocytosed by macrophages caused comparable cytotoxicity to long fibers at 24 h when compared at similar number-based dose (Goodglick and Kane, 1990). There is also an indication that asbestos particles shorter than 5 μm may be critical for health outcomes from the in vivo retention and translocation standpoints (Miserocchi et al., 2008; Adib et al., 2013; Dodson et al., 2003). No study, however, has utilized well-characterized respirable EMP preparations.

Numerous cell populations are involved in asbestos-related pathology, with resident alveolar macrophages being one of the primary mediators of the host immune response. Their depletion during asbestos-induced lung disease exacerbates fibrosis and worsens overall prognosis (Joshi et al., 2020). Accordingly, macrophage responses, including patterns of cell damage, cytokines, chemokines, and changes in gene expression could be related to the specific features of the fibers, meaning toxicological studies must go hand in hand with detailed EMP characterization. Macrophage-based in vitro systems are uniquely important for the EMP hazard prediction (Oberdorster and Graham, 2018). They can also help minimize the comprehensive toxicity testing based on long-term animal studies and epidemiological evaluations of each type of EMP.

We hypothesized that alveolar macrophage responses (response defined as a change from the normal state) to respirable non-asbestiform EMPs that fall in the WHO "critical" fiber range are similar to asbestiform variety of the same minerals, especially when compared at equal surface area or number, rather than mass. To test this hypothesis, we exposed primary mouse alveolar macrophage-like cells (MPI cells) for 24 h to preparations of asbestiform (asbestos) and non-asbestiform (cleavage fragments) respirable EMPs, at doses equivalent for total mass, surface area, or number of the particles with length $>$ 5 μm and aspect ratio $>$ 3:1, and evaluated the cytotoxicity, DNA damage, cytokine secretion and differential gene expression.

2. Methods

2.1. Particle preparation and characterization

Specific particles that were investigated as part of this study included non-asbestiform tremolite, prepared by the U.S. Bureau of Mines for the National Institute of Environmental Health Sciences (NIEHS) for use in oral ingestion studies (National Toxicology, 1990), Union Internationale Centre le Cancer (UICC) riebeckite asbestos (crocidolite), supplied by Research Triangle Institute (RTI International), non-asbestiform riebeckite obtained by NIOSH from Pikes Peak in Colorado Springs, Colorado, and tremolite asbestos from Lone Pine, California, also provided by NIOSH. Sample preparation is described in detail in the supplementary material. Briefly, the bulk material was crushed by a hydraulic press, sieved, and ground by hand until sufficient amount of EMPs with the desired dimensions were observed under polarized light microscopy (PLM). For PLM counting purposes small aliquots were suspended in a mixture of deionized water and isopropanol and filtered through 0.45 μm mixed cellulose ester (MCE) filters. Particle characterization was performed using a Hitachi 7000 analytical electron microscope with AMT XR280 digital camera. Particles were measured at an on-screen magnification ranging from 4570× to 21,900×. Three TEM grids were prepared from each of the mineral samples. Each grid square analyzed was traversed from left to right. At least 700 particles were measured in each sample. Length and width measurements in microns and aspect ratio for each particle were registered. From that data approximate surface areas of individual particles were calculated using the formula 4 * (*length* * *width*) + 2 * (*width* * *width*). EMP elemental composition was assessed using SEM coupled with the energy-dispersive X-ray spectroscopy (EDS).

2.2. Cell culture

The experiments were conducted in vitro and utilized alveolar macrophage–like cells, obtained and differentiated from the murine fetal livers (Max Planck Institute a.k.a. MPI cells) (Fejer et al., 2013).

MPI cells are phenotypically close to alveolar macrophages, can self-renew in culture, and respond to respirable particulates (Deville et al., 2020). MPI cell culture was a generous gift by Dr. J. Pestka from the University of Michigan, originally obtained from the fetal livers of C57BL/6 J mice following the standard protocol. Cells were cultured in Roswell Park Memorial Institute (RPMI) medium with 10% fetal Bovine Serum (FBS), 1% L-glutamine (HyClone), 1% penicillin-streptomycin mixture (HyClone), and 30 ng/ml of mouse recombinant GM-CSF (R&D Systems). Humidified incubator (Fisher Scientific) at 37 °C and an atmosphere of 5% *v*/v CO_2 was used. Cells were routinely passaged when reaching 75% confluence, using Accutase (Innovative Cell Technologies, San Diego, CA) detachment solution. Passages between 4 and 8 were used for the studies. Phenotypic profile of MPI cells was confirmed using flow cytometry as follows: cells at passage 5 were detached using Accutase, suspended in staining buffer and stained with fluorochrome-conjugated antibodies versus CD45 (Clone: 30-F11, BD), Siglec F (Clone: E50-2440, BD Horizon™), CD11c (Clone: N418, eBioscience™), CD64 (Clone: X54-5/7.1, Biolegend) and CD24 (Clone: M1/69, BD) (all obtained from Fischer Scientific, Pittsburgh, PA). Samples were run on Amnis FlowSight imaging flow cytometer (Luminex Corp., Austin, TX) and analyzed using IDEAS 6.2 software. Alveolar macrophage genotype was confirmed using the Mouse Cell Atlas (Suo et al., 2018) by uploading the raw counts from bulk Next Gen RNA Sequencing.

2.3. Treatment details

Dry EMP preparations were heated to 220 °C for 2 h to inactivate endotoxin. Endotoxin presence was further investigated in the stock suspensions using Limulus amebocyte lysate (LAL) chromogenic endpoint assay kit (Hycult biotech, Inc., Plymouth Meeting, PA). Stock particle suspensions were prepared in Ca^{2+}, Mg^{2+}-free phosphate-buffered saline (PBS, pH 7.4) at the concentrations of 1.0 mg/ml. The EMPs were serially diluted in phenol-free RPMI medium with 1% FBS, 1% penicillin/streptomycin and 30 ng/ml of GM-CSF (treatment medium) at appropriate concentrations. Immediately before dilution, stock suspensions were sonicated in a 20 kHz Q500 sonicator with 5.5″ cup horn (QSonica LLC, Newtown, CT). The settings were set to six pulses, ten seconds each, with five seconds intervals between, at 30% amplitude, for a total delivered energy of ~625 J/ml per sample.

The current consensus is that EMPs with greater than 5 μm lengths should be prioritized in terms of the possible health effects, thus for dosing we accounted for the number and total surface area of the fibers of sufficient length and greater than 3:1 aspect ratio, using the approach described in the Particle preparation section above. The importance of the surface area of the critical fibers parameter have been established by a number of robust and highly cited studies (Duncan et al., 2014; Davis et al., 1991; Aust et al., 2011; Mossman et al., 2011). The example of critical fiber number and surface area values per unit of mass (120 μg) is shown in Table 1. MPI cells, grown in 6-well and 96-well plates, were washed with PBS and treated with the mass-equivalent (9 μg/cm^2 for riebeckite asbestos and CF and 5 μg/cm^2 for tremolite asbestos and CF), fibers surface area-equivalent (9 and 40 μg/cm^2 for riebeckite asbestos and CF respectively, 5 and 60 μg/cm^2 for tremolite asbestos and CF respectively), and fibers number-equivalent (6 and 40 μg/cm^2 for riebeckite asbestos and CF respectively, 1.2 and 60 μg/cm^2 for tremolite asbestos and CF respectively) doses of asbestiform/non-asbestiform riebeckite or tremolite EMPs for 24 h. There were no equal mass comparisons between riebeckite and tremolite minerals, but 5 μg/cm^2 tremolite asbestos and 9 μg/cm^2 riebeckite asbestos doses had similar total surface areas of critical fibers between each other. The fiber number for all equivalent doses utilized in our study were within the number concentrations used in other studies and relevant to exposed workers' lifetime-accumulated number of fibers (Supplementary material).

Table 1
The total number and surface areas of particles in the test articles, including "critical" fibers, having length > 5 μm and aspect ratio of ≥3:1, per 120 μg of dry bulk preparations.

Per 120 μg	Total number		Total surface area of all particles, cm^2/g	Total surface area of critical fibers, cm^2/g
	Fibers	Non-fibers		
Tremolite	1.48E+07	4.68E+08	2.43E+04	2.02E+04
Riebeckite	4.88E+06	4.21E+08	1.15E+04	9.91E+03
Tremolite CF	2.83E+05	1.10E+06	2.94E+03	1.68E+03
Riebeckite CF	7.77E+05	3.88E+06	5.11E+03	2.47E+03

2.4. Cytotoxicity assessment

For cytotoxicity assessment MPI cells were plated at a density of 3×10^4 cells per well in 96-well microplates one day prior to EMP treatments. 24 h after the start of treatment, cell membrane damage was assessed using commercially available lactate dehydrogenase (LDH) assay (Pointe Scientific, Lincoln Park, MI) by monitoring the reduction of NAD+ in the presence of lactate in the supernatants at 340 nm in a Synergy H1 plate reader (Biotek, Winooski, VT). Multi-Tox Fluor kit (Promega, Madison, WI) was used to evaluate the viability following EMP treatment per the assay instructions. 1 μM staurosporine (Sigma-Aldrich, St. Louis, MO) was chosen as positive control, since apoptosis was suspected to be the major cell death mechanism following exposure to the studied EMPs. Staurosporine was also previously used in murine macrophage in vitro LDH and viability assays (Spencer et al., 2014). Cytotoxicity experiments were performed three times, with at least eight technical replicates (wells) per treatment per experiment.

2.5. Assessment of DNA double-strand breaks via 2-color flow cytometric analysis

Formation of double strand DNA breaks (DSB) triggers phosphorylation of the histone variant H2AX at Ser-139, producing γH2AX. By measuring the amount of phosphorylation, we can estimate the extent of DNA damage. MPI cells at passage six were seeded in 6-well plates at the density of 1×10^6 cells per well one day prior to EMP treatments. 24 h after the start of treatment, supernatants from each well were taken for the cytokine measurements, while cells were washed with PBS and detached using the Accutase detachment solution. After collection, 20 μl of cell suspension was taken for counting using Trypan Blue exclusion method on a Countess FL II automated cell counter, and the rest were centrifuged at 300 x*g*, and washed once with PBS. Cells were then fixed and permeabilized using FOXP3 Fix/Perm solution (Invitrogen, Carlsbad, CA), and stained with anti-Phospho-Histone H2A.X(Ser139) antibody conjugated with eFluor® 660 fluorophore (Invitrogen, Carlsbad, CA) together with Hoechst 33342 nuclear dye (Invitrogen, Carlsbad, CA) per supplied protocols. Samples were processed on an Amnis FlowSight imaging flow cytometer (Luminex Corp., Austin, TX) and analyzed using IDEAS 6.2 software. 50,000 cells per sample were collected for analysis. Tthe median Max Pixel intensity parameter in the cells exhibiting higher than threshold amount of γH2AX (greater than 98.5% of control cells) was recorded. 500 μM H_2O_2 treatment was used as a positive control. Sub-G1 cell populations were additionally evaluated as a marker of apoptosis/secondary necrosis. Gating strategy is visualized in Supplementary Fig. S2. Three technical replicates (three wells across three 6-well plates) per treatment were used.

2.6. Cytokine secretion in the supernatants

Cell supernatants from the 6-well plates used for γH2AX staining (see above) were collected and snap-frozen until the further analysis. Secreted cytokine profiles were determined in the supernatants using Bio-Plex Pro Mouse Cytokine 23-plex Assay on a Bio-Plex 200 Reader

(Bio-Rad Laboratories, Hercules, CA) following manufacturer's directions, with three technical replicates allocated per each of three wells per sample. Prior to measurements supernatant samples were centrifuged at 2500 *g*. Cytokine quantities was normalized per total number of live cells in each well at the collection time. For each cytokine, out of range (OOR)-low results were set equal to 80% of the minimum within-range value, while OOR-high results were set equal to 125% of the maximum within-range value, if applicable. Hierarchical clustering analysis of the secreted cytokines was performed using Clustvis (Metsalu and Vilo, 2015), with Euclidean distance similarity and Ward's clustering method.

2.7. Next generation RNA sequencing

A different set of cells was plated in 6-well plates and treated with an equivalent surface area of the critical fibers-based doses, with three replicates (wells) per each treatment group. 24 h post-exposure cells were washed with PBS, lysed with the TRIzol™ reagent (Invitrogen, Carlsbad, CA) and stored at −80 °C in RNAse/DNAse-free tubes for further analysis. RNA was purified using RNeasy MiniKits (Qiagen, Mississauga, ON, Canada) as described by the manufacturer, quantified using Thermo Scientific™ Nanodrop™ ND-1000 and qualified by agarose gel electrophoresis. The mRNA was enriched by oligo(dT) magnetic beads. Illumina kits were used for the RNA-seq library preparation, which included procedures of RNA fragmentation, random hexamer primed first strand cDNA synthesis, dUTP based second strand cDNA synthesis, end-repairing, A-tailing, adaptor ligation and library PCR amplification. Finally, the prepared RNA-seq libraries were qualified using Agilent 2100 Bioanalyzer (Agilent Technologies, Santa Clara, CA) and quantified by qPCR absolute quantification method. The sequencing was performed on Illumina NovaSeq 6000 (Illumina, San Diego, CA). The expression level (FPKM value) of known genes and transcripts were calculated using ballgown through the transcript abundances estimated with StringTie. Principal Component Analysis was performed with genes that have the ANOVA p value $\leq$0.05 on FPKM abundance estimations. The number of identified genes and transcripts per group was calculated based on the mean of FPKM in group $\geq$0.5. Genes showing expression changes of at least 1.5-fold in either direction compared to their controls, having $p < 0.05$ and q (false discovery rate adjusted p-value) $\leq$0.1 were considered significantly differentially expressed and were considered for further analysis. All gene expression data were uploaded to NCBI's Gene Expression Omnibus and are accessible via accession number GSE157922.

2.8. Enrichment of KEGG pathways and GO enrichment analysis

Pathway analysis for the differentially expressed genes was carried out based on the latest KEGG (Kyoto Encyclopedia of Genes and Genomes) database. The analysis allows users to determine whether the differentially expressed mRNAs are enriched in certain biological pathways. The p-values calculated by Fisher's exact test were used to estimate the statistical significance of the enrichment of the pathways between the two groups. A p value cutoff of <0.05 was considered significant. We also investigated whether specific Gene Ontology (GO) terms were more likely to be associated with the DEGs. A Fisher's exact test is used to estimate the statistical significance of such enrichment of terms between the two groups (EMP and control). The p-value denotes the significance of GO Term enrichment in the differentially expressed gene list. All analyses with the differentially expressed genes were performed in R, Python or shell environment for statistical computing and graphics.

2.9. Statistical analysis

Statistical analysis was performed using SigmaPlot 14.0 (San Jose, CA). Treatment related differences were evaluated using Student's t-test or one-way ANOVA, as appropriate. A $p < 0.05$ was considered to be statistically significant. Data are presented as Mean ± SE. Principal component analysis and hierarchical clustering analysis were performed using online tool (www.clustvis.org).

3. Results

3.1. Particle characteristics

Summary of the EMP size and dimensions is listed in Table 2. Detailed tables for every sample can be found in the Supplementary Materials (Supplementary Tables 1–4). Asbestos samples had smaller median widths and higher aspect ratios, compared to cleavage fragments, but median lengths of all samples were around 5 μm as seen on the size distribution charts (See Supplementary Material). Representative TEM photographs of the samples are shown in Fig. 1. The EDS analysis showed elemental signatures to be predominantly Si, Fe, Mg, Na, and O for riebeckite EMPs, and Si, Ca, Mg, and O with only trace Fe for tremolite particles (Fig. 2). Cu signal comes from the copper grids utilized in the process.

3.2. EMP cytotoxicity

Cytotoxicity was observed for all treatments at 24 h with the normalized ratio of viable-to-dead cells significantly decreasing to 90–70% of untreated controls (Fig. 3). The examples of light microscopy images of the MPI cells 24 h after treatment can be seen in Supplementary Fig. S1. Riebeckite cleavage fragments were less cytotoxic than asbestos at the equivalent mass doses, however significant difference between the growth habits was observed only for the equal mass doses of riebeckite (Fig. 3A.). At the equal mass, asbestiform EMPs clearly caused significantly greater LDH leakage (Fig. 4). For riebeckite EMPs, LDH leakage from the cells was similar at the calculated surface area equivalent doses (Fig. 4A). When treated with equal particle numbers, CF trended to have more pronounced cytotoxic effects, compared to respective asbestiform analogues, however never reaching statistical significance.

3.3. Relative amount of the γH2AX staining and nuclear staining analysis

Isolated particles were excluded from the analysis through initial size/aspect ratio scatterplot. Further, the imaging flow cytometry allows checking the visuals of every registered event. We spotted only several large enough isolated particles, all cleavage fragments, in the data collection gates among thousands of cells across all samples. Hoechst 33342 binding to the particles was negligent. Individual cell γH2AX signal was highest in asbestos-treated cells, specifically riebeckite asbestos. There was no difference between tremolite asbestos and CF treatments at number-equivalent dose. Cleavage fragments were not as efficient in inducing the H2AX phosphorylation in general (Fig. 5). Nuclear staining revealed increased number of cells found in the sub G-1

Table 2
Morphological characteristics of the studied EMPs, calculated from the detailed TEM analysis of at least 700 particles per sample. CF - cleavage fragments, A.R. – aspect ratio.

	Riebeckite	Tremolite	Riebeckite CF	Tremolite CF
Median length, μm	4.43	4.65	5.45	5.59
Length range (Min-Max), μm	0.67–63.2	0.61–55	0.96–23.7	0.7–33.7
Median width, μm	0.264	0.254	1.74	1.11
Width range (Min-Max), μm	0.03–3.26	0.02–2.14	0.14–6.58	0.01–13.4
Median A.R.	15.7	17.2	3.2	4.93
A.R. range (Min-Max)	2.7–636.4	2–362	1.12–18.5	1–126.07

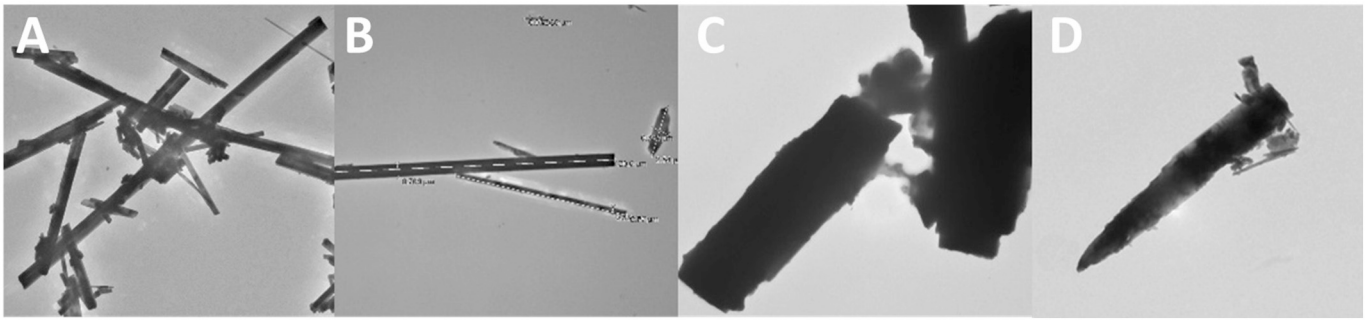

Fig. 1. Representative TEM photographs of riebeckite asbestos (A), tremolite asbestos (B), riebeckite cleavage fragments (C) and tremolite cleavage fragments (D); Scale bars correspond to 2 μm.

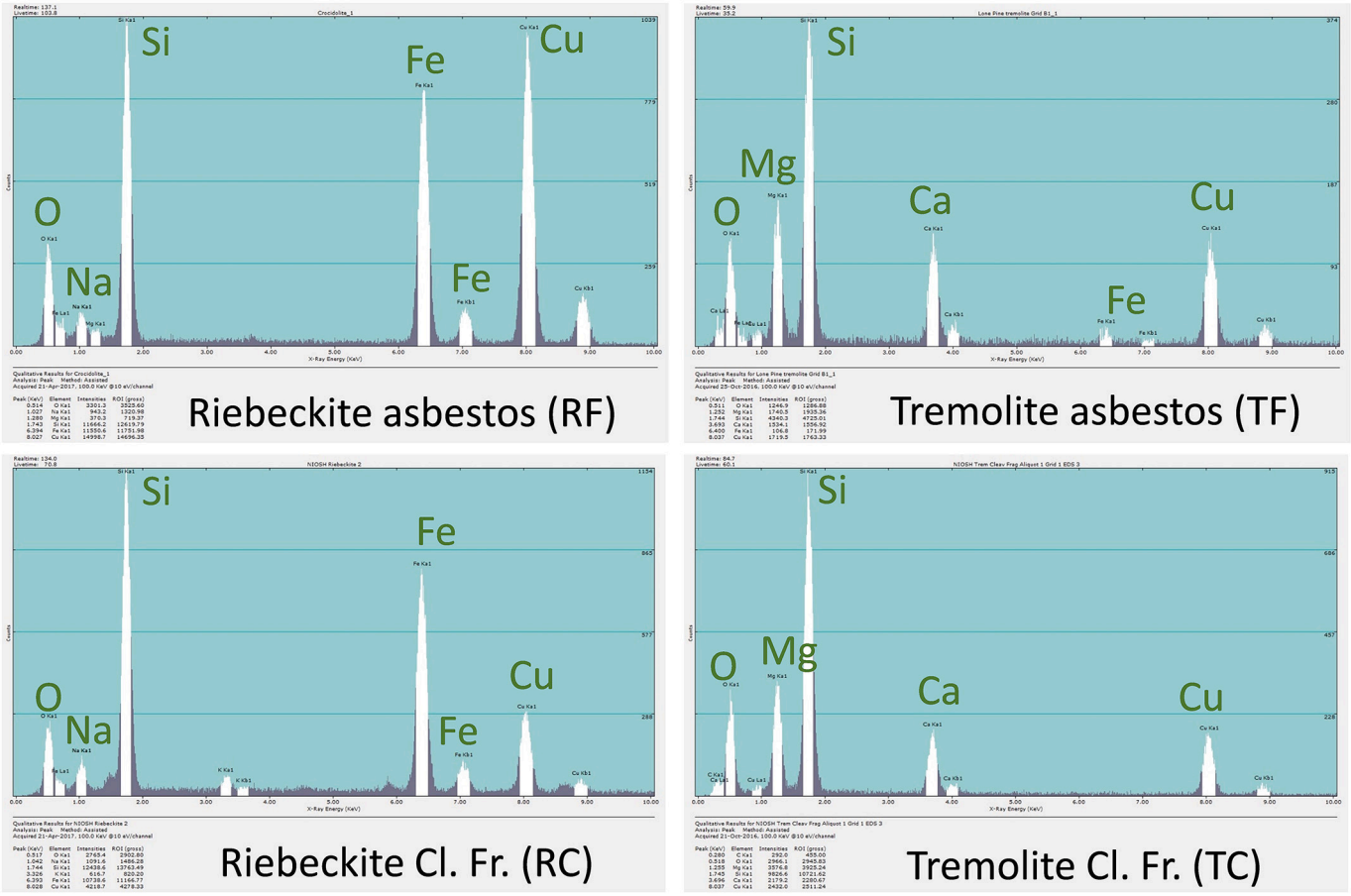

Fig. 2. Representative EDS spectra of the studied EMPs. The highest peaks have the associated element identifications. RF – riebeckite asbestos, RC – riebeckite cleavage fragments, TF – tremolite asbestos, TC – tremolite cleavage fragments.

region of the dot plots (Fig. 6, Supplementary Fig. S2) for riebeckite CF, tremolite CF, and riebeckite asbestos. Riebeckite CF had lower sub-G1 cells than riebeckite asbestos at mass-equivalent doses, and higher at surface area-equivalents. Tremolite asbestos treatment did not significantly increased the Sub-G1 population of cells compared to controls.

3.4. Cytokine secretion

All EMP treatments provoked significant secretion of IL-1α, MCP-1, MIP1α and MIP1β and KC (mouse analog of IL-8), but not other cytokines, such as IL-6 or TNF-α (Supplementary file Cytokine_Data.xlsx). Hierarchical cluster analysis of the cytokine/chemokine secretion was performed for the cytokines/chemokines, showing significant difference ($p < 0.05$) in at least 3 different treatments, compared to respective controls: IL-1α, MCP-1, MIP1α, MIP1β and KC cytokines, and showed close clustering for the surface area and fiber number equivalent treatments (Fig. 7).

3.5. Next generation RNA sequencing

Principal component analysis (PCA) showed a distinguishable gene expression profiling among the samples (Fig. 8). PCA also demonstrated expected grouping among replicates within samples and also sample groups with different treatment spread across the first two PC dimensions. The Pearson R2 correlation of gene expression between replicates was well over 0.92 (Supplementary Fig. S3) suggesting an inter-

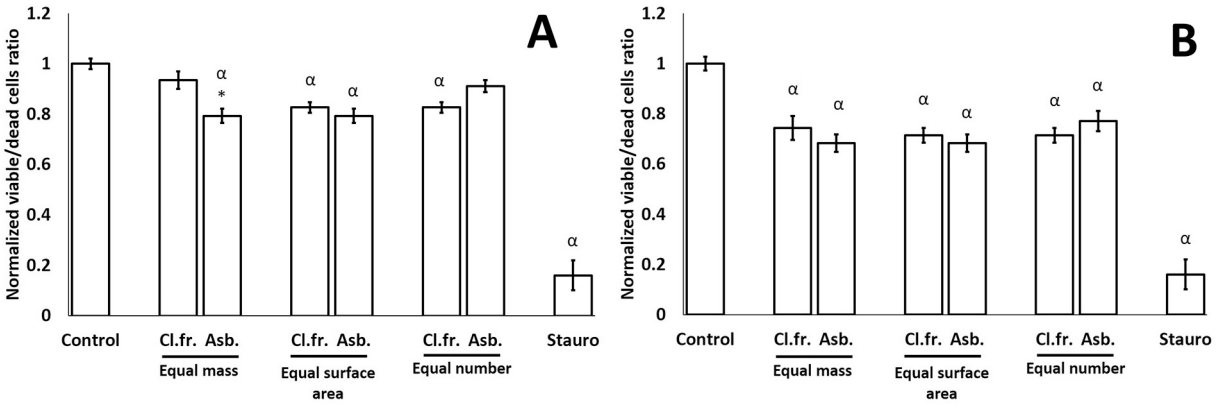

Fig. 3. Normalized viable/dead cells ratios, 24 h exposure to riebeckite (A) or tremolite (B) EMPs. Values are expressed as mean ± SEM from 3 independent experiments. Stauro – 1 μM of staurosporine. Equal mass: 9 μg/cm^2 for both riebeckite asbestos and cleavage fragments (CF); 5 μg/cm^2 for both tremolite asbestos and CF; Equal surface area of critical fibers: 9 and 40 μg/cm^2 for riebeckite asbestos and CF, 5 and 60 μg/cm^2 for tremolite asbestos and CF; Equal number: 6 and 40 μg/cm^2 for riebeckite asbestos and CF, 1.2 and 60 μg/cm^2 for tremolite asbestos and CF. $^{\alpha}p < 0.05$ vs. control; * $p < 0.05$ vs. cleavage fragments equivalent.

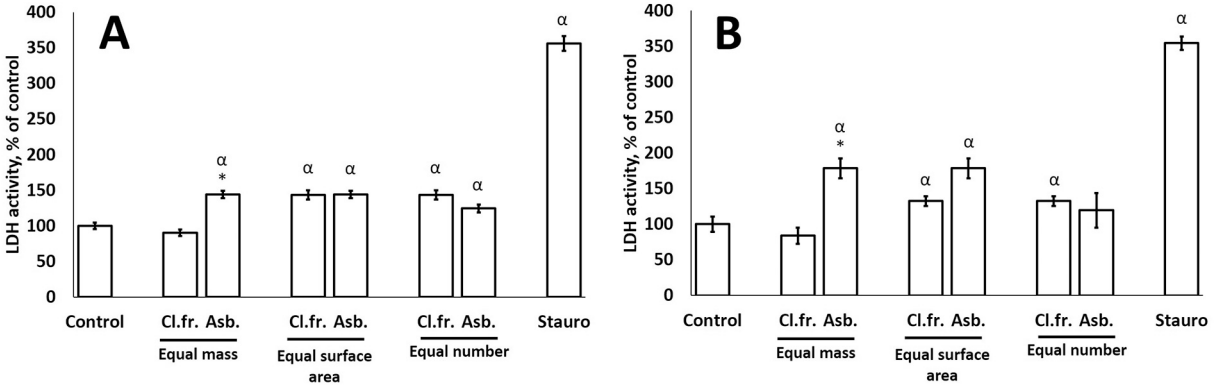

Fig. 4. LDH activity in the supernatant, as percentage of untreated cell values. 24 h exposure to riebeckite (A) or tremolite (B) EMPs. Values are expressed as mean ± SEM from 3 independent experiments. Stauro – 1 μM of staurosporine. Equal mass: 9 μg/cm^2 for both riebeckite asbestos and cleavage fragments (CF); 5 μg/cm^2 for both tremolite asbestos and CF; Equal surface area of critical fibers: 9 and 40 μg/cm^2 for riebeckite asbestos and CF, 5 and 60 μg/cm^2 for tremolite asbestos and CF; Equal number: 6 and 40 μg/cm^2 for riebeckite asbestos and CF, 1.2 and 60 μg/cm^2 for tremolite asbestos and CF. $^{\alpha}$ $p < 0.05$ vs. control; * $p < 0.05$ vs. cleavage fragments equivalent.

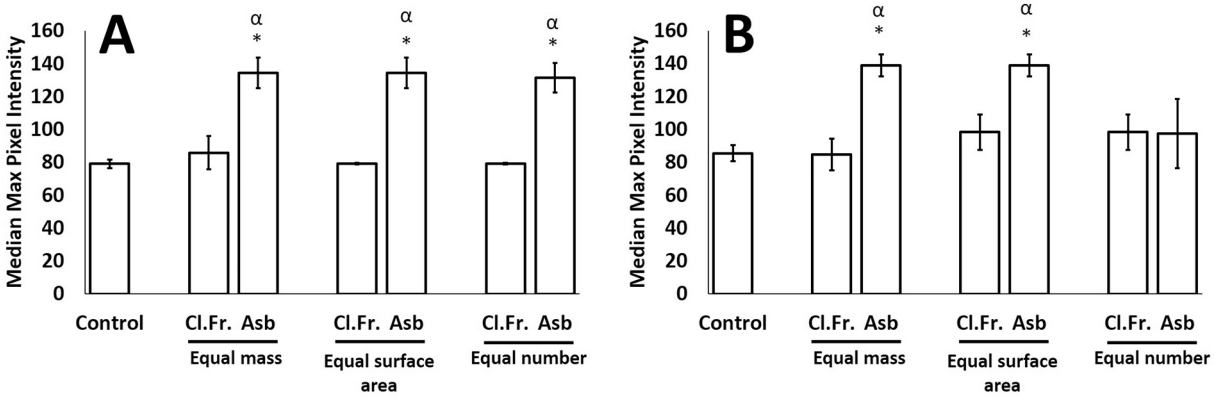

Fig. 5. Median Max Pixel intensity (arbitrary units) of the γH2AX fluorescence staining in the signal gate, 24 h exposure to riebeckite (A) or tremolite (B). Values are expressed as mean of three biological replicates ± SEM. Equal mass: 9 μg/cm^2 for both riebeckite asbestos and cleavage fragments (CF); 5 μg/cm^2 for both tremolite asbestos and CF; Equal surface area of critical fibers: 9 and 40 μg/cm^2 for riebeckite asbestos and CF, 5 and 60 μg/cm^2 for tremolite asbestos and CF; Equal number: 6 and 40 μg/cm^2 for riebeckite asbestos and CF, 1.2 and 60 μg/cm^2 for tremolite asbestos and CF. $^{\alpha}$ $p < 0.05$ vs. control; * $p < 0.05$ vs. cleavage fragments equivalent.

and intragroup variablity, consistent with each group belonging to the same cell and exposure type.

Detailed comparative analysis of all differentially expressed genes (DEG) revealed 492↑/302↓, 374↑/220↓, 224↑/70↓ or 258↑/118↓ up (↑)/down (↓) regulated genes with a significant fold change ≥ ±1.5 in response to riebeckite asbestos, riebeckite CF, tremolite asbestos and

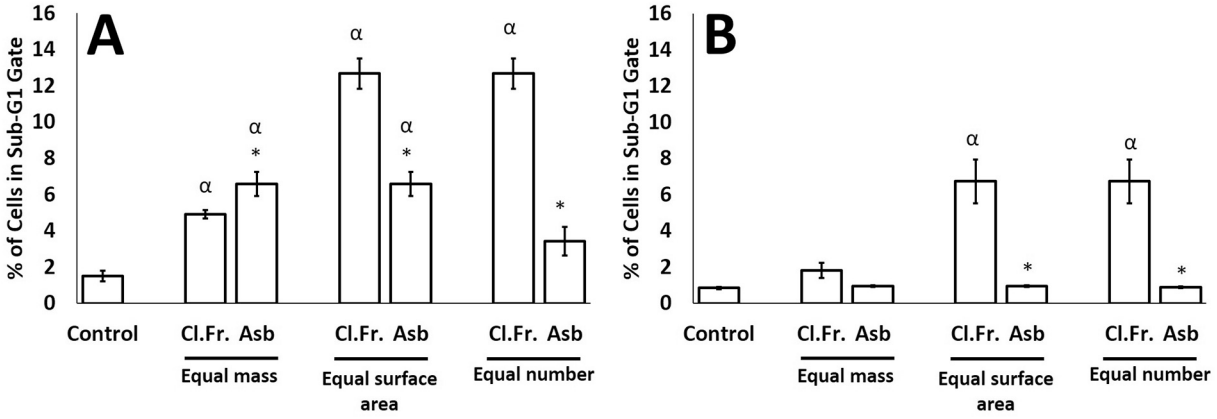

Fig. 6. % of cells in the sub-G1 gate, relative to total cells, 24 h exposure to riebeckite (A) or tremolite (B). Values are expressed as mean of three biological replicates ±SEM. Equal mass: 9 μg/cm^2 for both riebeckite asbestos and cleavage fragments (CF); 5 μg/cm^2 for both tremolite asbestos and CF; Equal surface area of critical fibers: 9 and 40 μg/cm^2 for riebeckite asbestos and CF, 5 and 60 μg/cm^2 for tremolite asbestos and CF; Equal number: 6 and 40 μg/cm^2 for riebeckite asbestos and CF, 1.2 and 60 μg/cm^2 for tremolite asbestos and CF. $^{\alpha}$ $p < 0.05$ vs. control; * $p < 0.05$ vs. cleavage fragments equivalent.

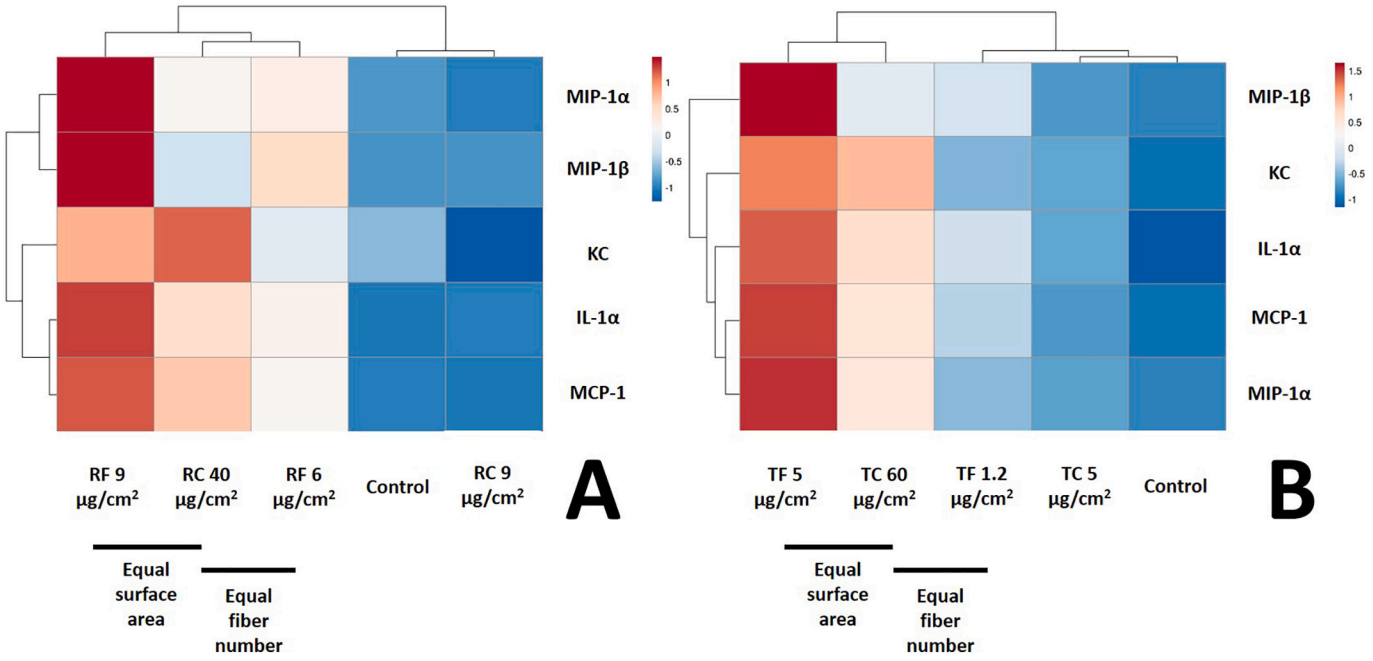

Fig. 7. Hierarachical clustering of the secreted cytokine profiles for the MPI cells exposeed to riebeckite (A) or tremolite (B) EMPs. RF – riebeckite asbestos, RC – riebeckite cleavage fragments, TF – tremolite asbestos, TC – tremolite cleavage fragments. Rows are centered; unit variance scaling is applied to rows. Both rows and columns are clustered using Euclidean distance and Ward linkage. Heatmap reflects unit variance.

tremolite CF, respectively (Fig. 9). There were more uniquely dysregulated genes common for the riebeckite EMP samples (198), compared to tremolite exposures (10). Among the top 10 DEGs, all 4 materials upregulated 5 (*H2-M2, Inhba, Cfb, Acp5, Ear2*) and down-regulated 5 (*Cfh, Clec4a, Ifitm6, Sell, Clec12a*) common genes, with several others common for 2 or 3 of the EMPs (Table 3). *H2-M2* (MHC-II) was the most upregulated gene. *Acod1* was highly upregulated in asbestos and less so in cleavage fragments. Complement factors B (*Cfb*) and H (*Cfh*) had opposite regulation status. The full list of DEGs is available in Supplementary Materials.

3.6. KEGG pathway enrichment analysis

Pathways analysis of DEGs following 24 h of exposure to riebeckite asbestos, riebeckite CF, tremolite asbestos and tremolite CF predicted the involvement of a total of 61, 21, 44 and 25 pathways ($p < 0.05$), respectively. 11 of them were common to all exposure groups (Supplementary file KEGG.xlsx). Those were associated with the immune cell differentiation, inflammation, complement activation, cancer, and granulomatous lesions. *Cytokine-cytokine receptor interaction* was one of the most uniformly enriched pathways across all groups. *NF-kB signaling, and Phagosome* were enriched for all groups except riebeckite CF. *Th1 and Th2 cell differentiation* was exclusive for asbestiform EMPs. Riebeckite asbestos had the most number of uniquely enriched pathways, including *Regulation of actin cytoskeleton*, *Fc gamma R-mediated phagocytosis*, *Galactose metabolism*, *Natural killer cell mediated cytotoxicity*, *Lysosome*, *B cell receptor signaling pathway*, *MAPK signaling pathway*, *HIF-1 signaling pathway*, and *Ferroptosis*. Pathway associated with *NOD-like receptor signaling* was uniquely represented only upon tremolite asbestos exposure. *JAK-STAT* and *PPAR* signaling pathways were unique for riebeckite EMPs and tremolite CF, while *PI3K-Akt signaling pathways* was shared only by riebeckite samples. There was also a marked difference

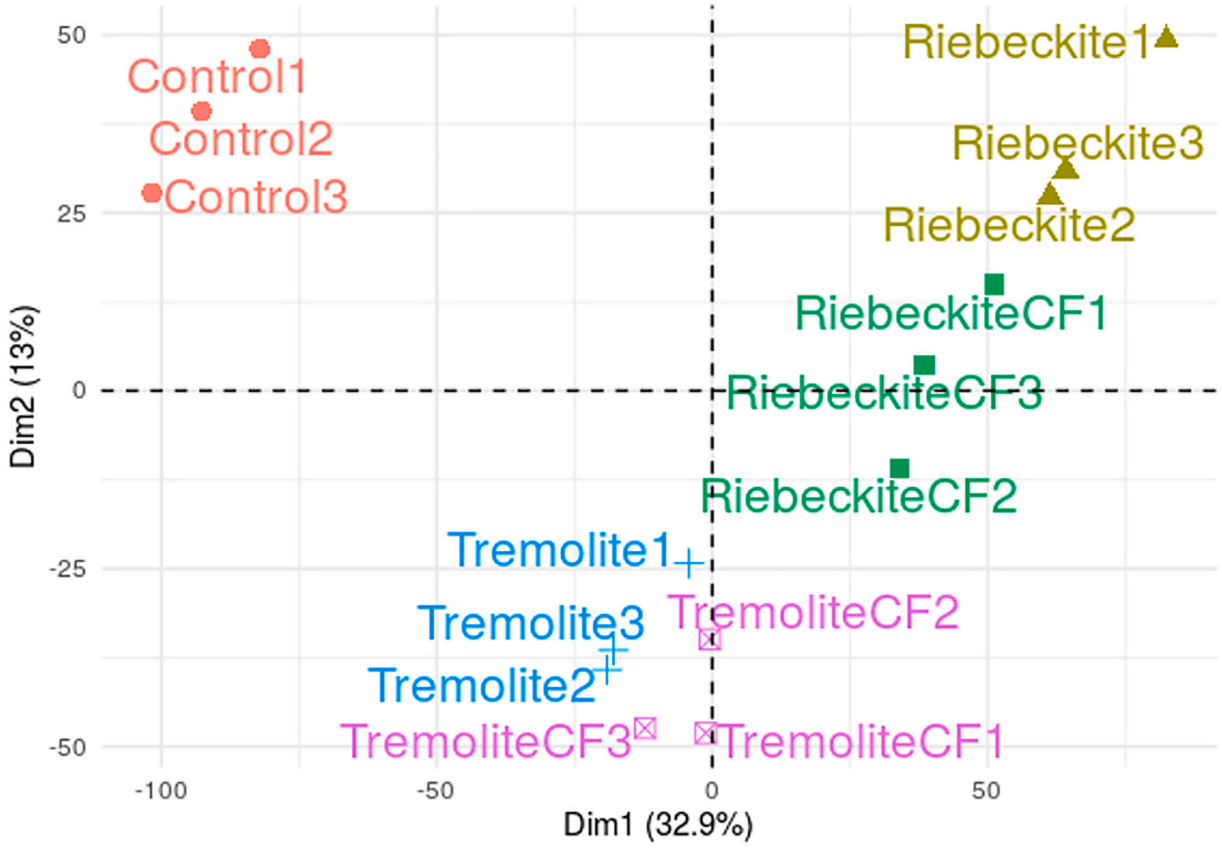

Fig. 8. Principal component analysis of the gene expression profiles in MPI cells, treated with critical fibers' surface area-equivalent doses of riebeckite and tremolite asbestiform and non-asbetiform EMPs. CF – cleavage fragments.

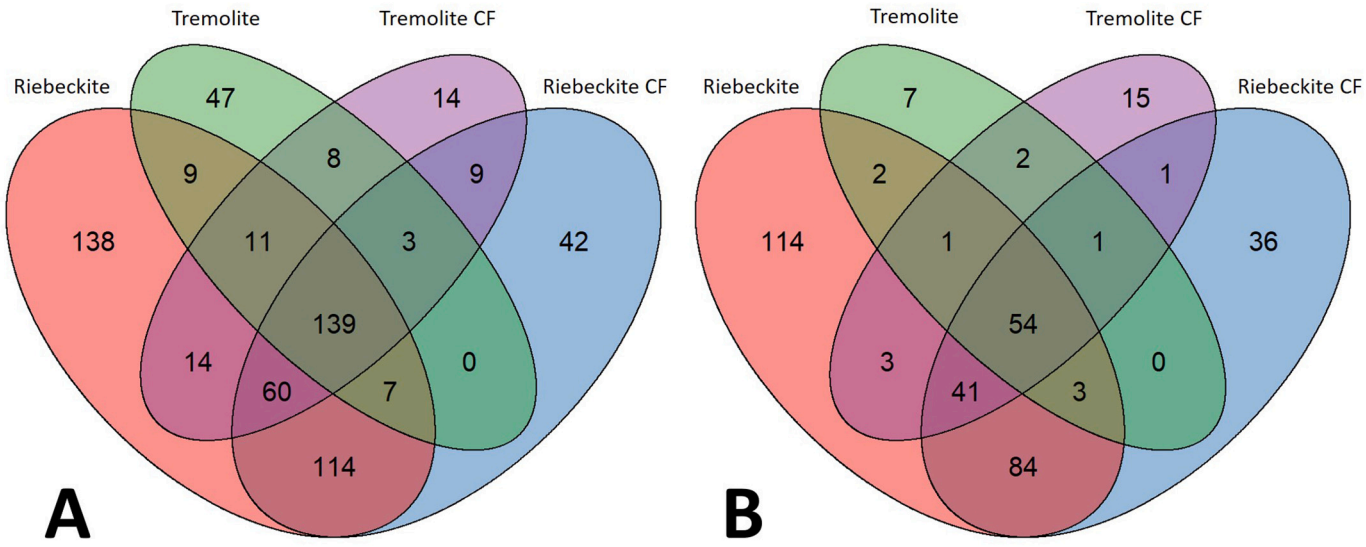

Fig. 9. Venn Diagrams for upregulated (A) and downregulated genes (B) of MIP cells, treated with critical fibers' surface area-equivalent doses of riebeckite and tremolite asbestiform and non-asbetiform EMPs, compared to untreated cells.

between asbestiform and non-asbestiform riebeckite, the former having 41 enriched pathways, not registered in CF. There were also notable differences between tremolite asbestos and CF, and the only common term unique for tremolite mineral EMPs was *Transcriptional misregulation in cancer*.

3.7. Gene ontology term enrichment analysis

GO analysis revealed significant enrichment of the upregulated DEGs in a lot of specific biological processes (BP), most of them tied with the immune responses (Supplementary file GOBP.xlsx). Asbestiform EMPs had overall higher enrichment scores compared to their non-asbestiform counterparts. Tremolite asbestos and cleavage fragments had more

Table 3
The top 10 most significantly up- and down-regulated genes. Bold font indicates dysregulated genes common for all treatments. CF - cleavage fragments.

Gene Symbol			
Riebeckite	**Riebeckite CF**	**Tremolite**	**Tremolite CF**
Top 10 UP Regulated Genes (Log_2 Fold Change)			
***H2-m2* (4.783)**	***H2-m2* (3.406)**	***H2-m2* (3.969)**	***H2-m2* (2.837)**
Acod1 (3.622)	***Ear2* (3.157)**	***Cfb* (2.575)**	***Inhba* (2.723)**
***Inhba* (3.475)**	***Acp5* (2.908)**	*Acod1* (2.503)	***Ear2* (2.488)**
***Cfb* (3.396)**	***Cfb* (2.688)**	***Inhba* (2.415)**	*Krt79* (2.428)
***Acp5* (3.186)**	***Inhba* (2.614)**	***Ear2* (2.321)**	***Cfb* (2.298)**
Hp (2.846)	*Krt79* (2.588)	*Tmsb15b2* (1.948)	*Tgfbi* (2.009)
Slc6a12 (2.776)	*Cxcr2* (2.506)	*Tnfrsf9* (1.913)	*Serpine1* (1.974)
***Ear2* (2.766)**	*Siglec8* (2.274)	***Acp5* (1.839)**	*Mmp12* (1.816)
Krt79 (2.641)	*Serpine1* (2.206)	*Il7r* (1.826)	***Acp5* (1.792)**
Pdpn (2.544)	*Hp* (2.196)	*Emp1* (1.626)	*Pdpn* (1.791)
Top 10 DOWN Regulated Genes (Log_2 Fold Change)			
***Cfh* (−2.616)**	***Cfh* (−2.423)**	**Ifitm6 (−1.979)**	***Cfh* (−2.132)**
Adgre4 (−2.330)	*Adgre4* (−2.253)	***Cfh* (−1.898)**	***Ifitm6* (−2.085)**
***Clec4a3* (−2.254)**	***Ifitm6* (−2.077)**	***Sell* (−1.784)**	***Sell* (−1.860)**
***Ifitm6* (−2.184)**	***Sell* (−1.926)**	*Pram1* (−1.431)	*Pram1* (−1.600)
Ms4a8 (−2.128)	*Ch25h* (−1.911)	*F5* (−1.109)	*Adgre4* (−1.536)
Pram1 (−2.123)	*Emilin2* (−1.870)	*Tarm1* (−1.105)	***Clec12a* (−1.373)**
***Sell* (−1.949)**	*Olfm1* (−1.835)	***Clec4a3* (−1.102)**	*Ccn3* (−1.367)
Elovl6 (−1.904)	***Clec12a* (−1.794)**	*Gda* (−1.078)	***Clec4a3* (−1.345)**
Olfm1 (−1.770)	***Clec4a3* (−1.785)**	***Clec12a* (−1.064)**	*Ccnd1* (−1.271)
***Clec12a* (−1.767)**	*Klf2* (−1.759)	*Cd300lg* (−1.000)	*Klk3* (−1.254)

distinctions between each other than corresponding riebeckite EMPs. Specific GO biological processes, having much larger scores for the riebeckite samples were those related to apoptosis (GO:0010942, GO:0043065, GO:0097190), *intracellular transport* (GO:0071702), *response to toxic substance* (GO:0009636) and others. Tremolite had distinctively enriched BPs related to innate immunity (GO:0002252, GO:0045087) and viral defense (GO:0009615, GO:0051607, GO:0045071 etc.).

4. Discussion

Epidemiology of asbestos-related diseases and biological effects of asbestos fibers have been extensively studied since mid-twentieth century, resulting in a firm belief, that "a worldwide ban of asbestos would eventually virtually eliminate its associated diseases" (Schraufnagel and Society, 2010; Vincenten et al., 2017). Still, decades after becoming known to general public, conditions caused by asbestos exposures contribute most to the global occupational cancer burden and are responsible for the increasing mortality for occupational respiratory diseases (De Matteis et al., 2017), with 243,000 deaths attributable to asbestos in 2017 worldwide (Collaborators, 2018). In addition, while in vitro studies provided important information on asbestos-induced cyto- and genotoxicity, the essential knowledge of the significance and role of different features and characteristics of fibers, that define responses, is still missing.

There currently is a consensus that among critical determinants of the fibers' pathogenicity are their respirability (ability to deposit into the deep lung), geometric dimensions (Castranova et al., 1996), durability and surface reactivity (Lippmann, 2014). The latter is important for toxic effects due to the presence of reactive sites on EMP surface, which was reviewed extensively elsewhere (Aust et al., 2011). There is evidence that surface properties of asbestiform and non-asbestiform habits are quite similar for respective riebeckite and tremolite mineral (Andreozzi et al., 2017; Schiller et al., 1980). Whether growth habit itself is a determinant of EMP toxicity is the critical question that exists in the field of fiber toxicology. There were very limited efforts in elucidating the potential determinants of toxicity of non-asbestiform EMPs, with the general opinion leaning towards their non-toxic nature (Mossman, 2008). One of the major issues with the studies so far was inadequate preparation and characterization of EMPs, which lead to comparisons between vastly different asbestiform and non-asbestiform populations. In our study we: 1) attempted to refine the treatment approach by utilizing pre-made respirable asbestiform and non-asbestiform EMP formulations with the specific dimensional parameters, 2) included three dosing approaches: equivalent mass, surface area and particle number of the critical fibers, and 3) used relevant cell model by employing MPI cells, that are phenotypically close to alveolar macrophages (allowing us to forego using multiple animals for isolating alveolar macrophages from bronchoalveolar lavage). Fiber numbers for all equivalent doses utilized in our study were well within the number concentrations used in other studies and are within the exposed workers' lifetime-accumulated number of fibers (Supplementary material). We were not aiming at elucidating the precise mechanisms of asbestos-induced lung disease, due to its complexity and model limitations (Kamp and Weitzman, 1999).

Particle dimensions are important due to their established role in fiber toxicity paradigm. In case of human asbestos exposures, thinner fibers (< 0.1 μm thick) are associated with pleural plaques and mesothelioma, whilst those having width 0.1–3 μm – with fibrosis and lung cancer (Lippmann, 1988). Lengthwise, 5 μm is considered a "critical" fiber length by the health agencies (World Health, 2000; Group, 2003). Our sample preparations included EMPs within respirable range, with median lengths close to 5 μm (see Supplementary materials for detailed distribution charts), and cumulative frequency of EMPs with diameter < 3 μm at ~90%. Although not part of this study aims, it is important to make parallels with the short vs. long asbestos fibers toxicity paradigm, especially since significantly more studies focused on the shorter vs. longer asbestos rather than asbestiform vs. non-asbestiform EMP comparisons. The earliest evidence led to a prevailing opinion that long asbestos fibers in vitro are more cytotoxic to macrophages than short ones (Goodglick and Kane, 1990). The situation can be quite different in vivo, however, since EMPs longer than 20 μm rarely penetrates deep into the alveolar region. Thus, in vitro studies utilizing non-respirable EMPs should be evaluated having in mind this serious limitation. For non-fibrogenic fibers Castranova et al. found that short and thin glass fibers are more cytotoxic than thick and long (Castranova et al., 1996) while Padmore et al. discovered that shorter fibers are less potent in inducing the inflammatory responses (Padmore et al., 2017). However, both short and long riebeckite asbestos fibers were able to induce H_20_2 production by macrophages and cause cell death (Goodglick and Kane, 1990).

Airborne particles deposited in the airways and respiratory compartments can be recognized and cleared by macrophages – innate immune cells with a range of molecular tools to deal with newcomers, be it microorganisms, inorganic dust or EMPs (Laskin et al., 2015). MPI cells have been utilized before to assess the alveolar macrophage response to infectious agents, such as *P. aeruginosa* and *S. pneumoniae* (Bastaert et al., 2018), *M. tuberculosis* (Woo et al., *2018*), *B. thailandensis* (Chen et al., 2019), and adenoviruses (Stichling et al., 2018) as well as nanoparticles (Deville et al., 2020). Previous functional study revealed that phagocytosis of fibrous particles, even longer than the cell itself, does not lead to the immediate loss of membrane integrity and death in macrophages, but pulling the fiber out (by other macrophage, for instance) does (Ishida et al., 2019). In our case we noticed a uniform decrease in the ratio of live/dead cells across the treatment groups, except the lower dose of riebeckite CF (mass-equivalent to riebeckite asbestos). At the same time, there was a significant increase in the LDH leaked from the cells, which was similar for riebeckite CF and asbestos if compared at the calculated surface area- and particle number-equivalent doses. Despite statistically significant decrease in the ratio of viable to dead cells for both higher and lower doses, the lower tremolite CF dose (5 $\mu g/cm^2$) did

not increased the LDH activity in supernatants. The difference may have to do with the excessive LDH leakage from the cells that were not yet dead in the other treatment groups. The cytotoxicity methods utilized, does not discriminate between necrosis and the consequences of a programmed cell death – apoptosis (Chan et al., 2013).

Differences between AM responses to riebeckite and tremolite can be approached by first looking at the redox behavior of respective minerals. EDS analysis confirmed the abundance of iron in riebeckite samples, but only a very small amount in tremolite asbestos and no detectable iron in tremolite CF. However, previously it was found that both riebeckite and tremolite fibers exhibit sustained surface reactivity, and in both studied minerals free radical production does not depend on total iron content, but rather on specific Fe^{2+} and Fe^{3+} sites on the surface (Andreozzi et al., 2017). Upon incubation with H_2O_2 – simulating the lysosomal conditions – hydroxyl radical yield from tremolite significantly drops by 24 h, as opposed to significant increase in riebeckite fibers, but sustained radical reactivity of tremolite continues (especially the $COO^- \bullet$ production) for quite a long time (Andreozzi et al., 2017). Increased genotoxicity of riebeckite over tremolite was previously observed in A549 cells (Pacella et al., 2012), but not in macrophages, which are capable of more prominent "oxidative bursts". To look deeper into the particle-specific cellular responses, we decided to measure the extent of DNA damage. Asbestos exposures had long been found causing double-strand DNA breaks (DSBs), mostly through mechanisms involving redox stress (Okayasu et al., 1999; Msiska et al., 2010; Marczynski et al., 1994; Moyer et al., 1994). DSBs are the most deleterious DNA lesions, which, if left unrepaired, may have severe consequences for cell survival, as they lead to chromosome aberrations, genomic instability, or cell death. Cells respond to DNA damage by activating the so-called DNA damage response (DDR), a complex molecular mechanism developed to detect and repair DNA damage. The formation of DSBs triggers activation of many factors, including phosphorylation of the histone variant H2AX, producing γH2AX. By measuring the amount of phosphorylation, we can estimate the extent of DDR. It should be noted, however, that H2AX phosphorylation also occurs under basal conditions, and can increase, for example during the cell division. There was a clear surge in median γH2AX signal in the asbestos-treated cells, compared to control and cleavage fragments, except for the lower dose of tremolite (equivalent for particle number to respective cleavage fragments). Equal surface area did not play role in this case. The plausible explanation being that relatively small but potent population of asbestiform EMPs, longer than 20 μm (about 5% in riebeckite and 4% in tremolite asbestos samples), can cause the most deleterious lesions or affect the DNA repair processes more severely (Levresse et al., 2000). Cell apoptosis also leads to the formation of DSBs during the DNA fragmentation. In permeabilized cells, the fragmented 182 bp DNA multimers may leak outside, resulting in a reduced DNA population of cells (sub-G1 peak on a cell-cycle histogram). Analysis of the nuclear staining signal revealed increased sub-G1 populations for most of the treatments, more so in riebeckite EMPs, with cleavage fragments having the highest values. However, upon closer inspection (Supplementary Fig. S2), it can be seen that sub-G1 populations in CF samples are confined closer to G1 itself, which is characteristic of necrotic cells, and do not exhibit significant γH2AX signal, while in riebeckite asbestos the sub-G1 cells localize away from the G1, many of them having high γH2AX, which is characteristic of cells at different stages of programmed cell death (Wlodkowic et al., 2010; Darzynkiewicz et al., 1997). Substantial presence of apoptotic cells is further supplemented by the specific enrichment of GO BP terms related to apoptosis in riebeckite-treated cells. The combined results still do not allow us to make confident assumptions regarding the prevalent mode of death in each treatment case. More extensive testing, focusing specifically on the hallmarks of cell deaths is required, since alveolar macrophage apoptosis has been implicated in the development of pneumoconiosis (Borges et al., 2001) and asbestosis (Hamilton et al., 1996).

The "tolerant" nature of the AM majority prevents overreaction and excessive activation. That being said, AM population is not homogenous and includes genotypically and functionally different varieties. (Joshi et al., 2018; Holt, 1986; Alber et al., 2012). Not all of them are strictly immunosuppressive and as early as in 1996 researchers hypothesized that the disbalance of suppressive vs. reactive subtypes (i.e. caused by the excessive apoptosis of the former subtype) is what constitutes the development of lung disease (Hamilton et al., 1996). MPI cells themselves are more than capable of acute pro-inflammatory reaction to pathogens, such as live *M. tuberculosis* (Woo et al., *2018*). In our study, compared to basal conditions, EMP-treatments only slightly upregulated secretion of alarmins, such as IL-1α, and IL-1β, but not TNF-α or IL-6, while at the same time caused significant increase in chemokines (MIP-1a, MIP-1b, MCP-1 and KC). This was previously observed ex vivo as well where alveolar macrophage obtained from the healthy human volunteers secreted minuscule amount of cytokines compared to the blood monocytes from the same subjects, after stimulation with 4 different types of asbestos, which was attributed to the translational block (Geist et al., 2000). Hierarchical cluster analysis of the cytokine/chemokine secretion pattern showed close clustering for the surface area and particle number equivalent treatments, with significantly more chemokines secreted by asbestos-treated cells compared to cleavage fragments (Supplementary File Cytokine_Data.xlsx). Secretion of chemokines/chemoattractant proteins is a major event happening during cell-fiber interaction. KC in particular is responsible for neutrophils chemotaxis, which plays a major role in the asbestosis pathogenesis (Broser et al., 1996). Although important from the macrophage response standpoint, these results cannot be reliably translated into the in vivo settings, as shown by multiple studies that assessed the cytokine secretion profiles of the AMs. It is established that, in humans with asbestosis, alveolar macrophages secrete pro-inflammatory cytokines and are overresponsive to the other stimuli (Perkins et al., 1993; Holian et al., 1997). Driscoll et al. reported considerable IL-1 and TNF-α secretion by rat alveolar macrophages at day 3 post exposure to crocidolite, which decreased substantially on days 7, 14, and 28 (Driscoll et al., 1995). The increased cytokine secretion observed in humans and animals, however, has not been reproduced in vitro (Perkins et al., *1993*), just like in our study.

Detectable changes in macrophage gene expression happen within 6–24 h post-stimuli (Schneider et al., 2019), thus we performed the next generation RNA sequencing of the MPI cells 24 h post exposure to surface area-equivalent doses of riebeckite and tremolite EMPs to see if AM immediate transcriptional reprogramming patterns are intrinsic for different minerals and/or crystallization habit. We decided to go with the surface area-equivalency, since it was more uniformly predictive of cytotoxicity for both riebeckite and tremolite, than fiber number equivalent doses. RNAseq revealed that MPI cells responded to EMP treatment by upregulating a significant number of genes responsible for the acute phase response, inflammation, antigen processing etc. Riebeckite asbestos had the most significantly dysregulated genes compared to control, followed by riebeckite CF, tremolite asbestos and tremolite CF. Genes involved in iron handling, such as haptoglobin (*Hp*), ferritin light chain (*Ftl1*), and heme oxygenase 1 (*Hmox1*) were prevalently upregulated by riebeckite asbestos treatment, although we cannot reliably tie it up with the higher iron content in this mineral, for instance, it can be just the part of an acute response response, such as inhibiting the pro-inflammatory HMGB1 molecules (Yang et al., 2017). However, transcriptional upregulation of both ferritin and heme oxygenase 1 have been previously implicated in asbestos-related pathology (Ghio et al., 2008; Nagatomo et al., 2007). *Acod1* is a gene, which is upregulated in the macrophages upon a plethora of stimuli, and is co-regulated together by TNF-α and IFN-gamma (Degrandi et al., 2009). Complement factor B (*Cfb*) was significantly upregulated in all groups, while its competitor – complement factor H (*Cfh*) – downregulated. Downregulation of the *Cfh* can be related to the excessive NFkB and IL-1β signaling (through the microRNAs), seen across the samples. While it might be beneficial for the initial innate responses, sustained *Cfh* deficits

may eventually result in pathogenic complement activation, chronic inflammation and autoimmunity, all seen in human asbestos exposures (Alexander and Quigg, 2007). The role of *Cfh* in lung diseases is still not clear, however some lung cancers upregulate *Cfh* expression to avoid cell lysis through the complement activation (Cui et al., 2011). A set of *Ifit* genes (*ifit3*, *ifit1b*, *ifit2*) was uniquely upregulated only in tremolite asbestos-exposed cells. This is peculiar, since those are mostly induced by type I (IFN-α/β) and type III (IFN-λs) interferons whereas type II IFN (IFN-γ) is much less potent (Fensterl and Sen, 2015). Ifit proteins lack enzymatic activity but bind a variety of RNAs and other macromolecules, contributing to the viral defense. Both KEGG pathway and GO BP analysis also revealed several highly enriched virus response pathways in tremolite asbestos samples. Type I interferons play an important role in lung homeostasis and can downplay the immune-mediated pathology (Divangahi et al., 2015), which is important for chronic conditions, such as asbestosis, and was already confirmed for silicosis (Giordano et al., 2010). KEGG analysis revealed that both asbestiform and non-asbestiform riebeckite EMPs induced *JAK-STAT, PPAR*, and *PI3K-Akt signaling pathways*, which may signify the close intracellular response patterns to that particular mineral – something we have not observed in tremolite-treated cells. Nevertheless, riebeckite asbestos had 41 enriched pathways, not present in respective CFs, including those related to NF-kB and MAPK signaling, cell adhesion molecules, as well as phagosome/lysosome function. GO BP also revealed more sophisticated transcriptional response to riebeckite asbestos, compared to CF. The fact that *NOD-like receptor signaling* KEGG pathway was enriched only in tremolite also requires further attestation by the functional assays, since we have observed the same in our mouse experiment at 7 days post-treatment with tremolite, but not riebeckite (Yanamala et al., 2018).

Overall, magnitude and direction of the gene expression dysregulation was the highest in riebeckite asbestos-treated cells and followed the similar patterns for riebeckite asbestos and cleavage fragments but was quite divergent for tremolite polymorphs. Together with the cytotoxicity and cytokine secretion data, a pattern emerges, when if compared at the equivalent surface area of critical fibers, asbestiform and non-asbestiform EMP preparations show some similarity in how AMs respond to them in a short time-frame of 24 h (Fig. 10.). The similarity is more pronounced for the riebeckite mineral than for tremolite, which may have to do with the potential differences in surface reactivity. The observed AM response patterns align with the threshold paradigm outlined by Cox et al. (Cox Jr., 2018): individual cellular endpoints, such as membrane or even DNA damage cannot serve as reliable predictors of an outcome. The notable differences in cell responses to riebeckite vs. tremolite mineral EMPs, including respective cleavage fragments might have to do with the variable iron content, presence of silanol groups, particle opsonization by specific proteins etc. It is more likely that only upon accumulation of different signals and the overcoming of activation threshold, the specific outcome can be observed. The combinations of signals may as well be different for different minerals: based on our results, growth habit might play bigger role for ones (tremolite) and be a less significant determinant for others (riebeckite).

Studies in vitro, like ours, have intrinsic limitations, and cannot address all the complexity of interactions among tissues and organs, and do not account for the modifying effects of deposition patterns and clearance by mucociliary actions as well as contribution from biopersistence. Specialists in the field all agree that "…what happens at the lung level is based on a population of fibers getting to the deep part of the lung and not based on one EMP interacting with one lung cell" (Weill, 2018). Artificial approach to the sample preparation, although necessary for adequate comparisons, is not exactly representative of the typical human exposures. In in vivo settings, shorter EMPs, including non-asbestform mineral analogues can be cleared more easily, but it does not mean they are less potent in causing cell damage in the sustained exposure scenario. Further studies focusing on the EMP-evoked free radical production and time-resolved cell death are necessary to complement the results of this study.

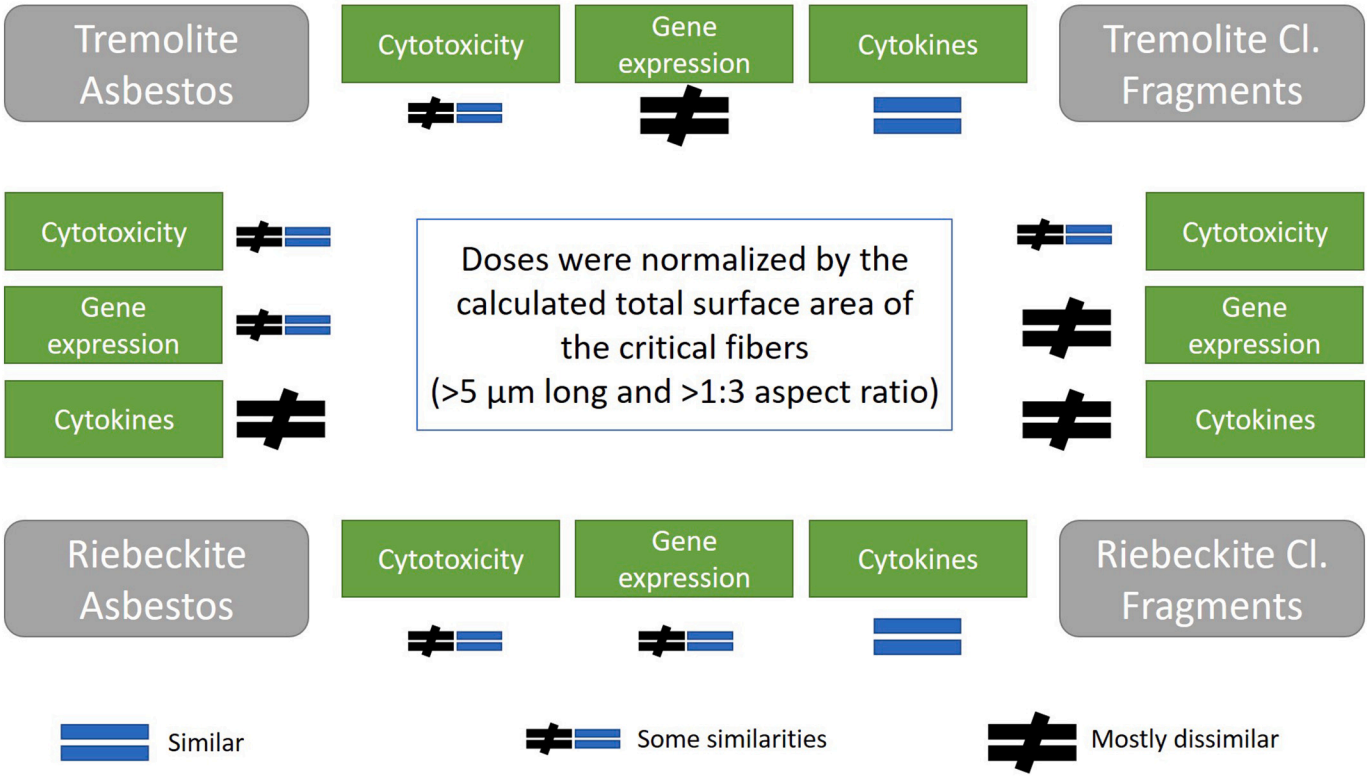

Fig. 10. Summary of the alveolar macrophages' responses to asbestiform and non-asbestiform EMPS if compared at the critical fibers' surface area-equivalent doses.

5. Conclusions

Our study is the first one that attempted to determine the toxicological profiles of comparable asbestiform and non-asbestiform EMPs populations in vitro, utilizing different dose metrics in a relevant alveolar macrophage model. We only partially confirmed the initial hypothesis. While equal mass-based doses resulted in markedly differential responses between asbestos and CF, at equal fiber surface area-based doses asbestos and corresponding CF had similar cytotoxic effects. However, when further comparing equivalent surface-area based treatments, there were distinct transcriptional reprogramming patterns and DNA damage, also specific for the mineral type, suggesting that asbestiform habit itself may be an important determinant for some minerals, like tremolite. Altogether, the accumulated evidence points us in the direction of the selective approach to choosing relevant EMP parameters for hazard identification step of risk assessment. Further understanding the factors and mechanisms by which EMP exert toxicity may lead to the emerging of new paradigm, where aside from determining the number of EMPs per volume of air, other parameters, such as surface area of the "critical" fibers should be accounted for. Future studies that account for that selective approach may help improve preventive and therapeutic measures for an ultimate goal of the reduction of pulmonary disease caused by EMPs. The results of such studies may contribute towards development of sampling and analytical methods that closely measure the characteristics important for toxicity, development of appropriate recommendations for worker protection and determination of criteria that could be used to predict the potential risk associated with exposure to any particular type of EMP. Finally, the results may help fill in knowledge gaps beyond EMPs – exposure to other elongate particles, including inorganic and organic manufactured materials.

Availability of supporting data

All data generated or analyzed during this study that is not included in this published article or its Supplementary materials is available from the corresponding author on reasonable request. Gene expression data is available in the NCBI's Gene Expression Omnibus, accessible via accession number GSE157922.

Disclaimer

The findings and conclusions in this report are those of the authors and do not necessarily represent the official position of the National Institute for Occupational Safety and Health, Centers for Disease Control and Prevention.

Funding

This work was supported by the NIOSH NORA 939051G grant.

Declaration of Competing Interest

The authors declare that they have no competing interests.

Acknowledgements

The authors thank Dr. T. Stueckle and Dr. R. Wells for their critical review of this manuscript.

Appendix A. Supplementary data

Supplementary data to this article can be found online at https://doi.org/10.1016/j.taap.2020.115302.

References

Adib, G., et al., 2013. Short, fine and WHO asbestos fibers in the lungs of Quebec workers with an asbestos-related disease. Am. J. Ind. Med. 56 (9), 1001–1014.
Alber, A., et al., 2012. The role of macrophages in healing the wounded lung. Int. J. Exp. Pathol. 93 (4), 243–251.
Alexander, J.J., Quigg, R.J., 2007. The simple design of complement factor H: looks can be deceiving. Mol. Immunol. 44 (1–3), 123–132.
Allen, E.M., et al., 2015. Occupational exposures and lung cancer risk among Minnesota taconite mining workers. Occup. Environ. Med. 72 (9), 633–639.
Andreozzi, G.B., et al., 2017. Surface reactivity of amphibole asbestos: a comparison between crocidolite and tremolite. Sci. Rep. 7 (1), 14696.
Aust, A.E., Cook, P.M., Dodson, R.F., 2011. Morphological and chemical mechanisms of elongated mineral particle toxicities. J Toxicol Environ Health B Crit Rev 14 (1–4), 40–75.
Baron, P.A., 2001. Measurement of airborne fibers: a review. Ind. Health 39 (2), 39–50.
Bastaert, F., et al., 2018. Pseudomonas aeruginosa LasB subverts alveolar macrophage activity by interfering with bacterial killing through downregulation of innate immune defense, reactive oxygen species generation, and complement activation. Front. Immunol. 9, 1675.
Belluso, E., et al., 2017. Crystal habit of mineral fibres, in Mineral Fibres: Crystal Chemistry, Chemical-Physical Properties, Biological Interaction and Toxicity. Mineralogical Society of Great Britain and Ireland, p. 0.
Berman, D.W., Crump, K.S., 2008. A meta-analysis of asbestos-related cancer risk that addresses fiber size and mineral type. Crit. Rev. Toxicol. 38 (Suppl. 1), 49–73.
Berman, D.W., Hibbs, P., Lippmann, M., 2018. Proceedings of the the Monticello Conference on Elongated Mineral Particles. Session III: Human exposure, effects & risk. Toxicol. Appl. Pharmacol. 361, 145–148.
Borges, V.M., et al., 2001. Fas ligand triggers pulmonary silicosis. J. Exp. Med. 194 (2), 155–164.
Broser, M., et al., 1996. Elevated interleukin-8 in the alveolitis of individuals with asbestos exposure. Int. Arch. Occup. Environ. Health 68 (2), 109–114.
Bugge, M.D., et al., 2012. Lung cancer incidence among Norwegian silicon carbide industry workers: associations with particulate exposure factors. Occup. Environ. Med. 69 (8), 527–533.
Castranova, V., et al., 1994. Comparative cytotoxic effects of crocidolite and its non-asbestiform polymorph on rat alveolar macrophages. Ann. Occupat. Hygiene 38 (inhaled_particles_VII), 665–673.
Castranova, V., et al., 1996. In vitro effects of large and small glass fibers on rat alveolar macrophages. J. Toxicol. Environ. Health 49 (4), 357–369.
Chan, F.K., Moriwaki, K., De Rosa, M.J., 2013. Detection of necrosis by release of lactate dehydrogenase activity. Methods Mol. Biol. 979, 65–70.
Chen, J., et al., 2019. Glycan targeted polymeric antibiotic prodrugs for alveolar macrophage infections. Biomaterials 195, 38–50.
Collaborators, G.B.D.R.F., 2018. Global, regional, and national comparative risk assessment of 84 behavioural, environmental and occupational, and metabolic risks or clusters of risks for 195 countries and territories, 1990-2017: a systematic analysis for the global burden of disease study 2017. Lancet 392 (10159), 1923–1994.
Cox Jr., L.A.T., 2018. Biological mechanisms of non-linear dose-response for respirable mineral fibers. Toxicol. Appl. Pharmacol. 361, 137–144.
Cui, T., et al., 2011. Human complement factor H is a novel diagnostic marker for lung adenocarcinoma. Int. J. Oncol. 39 (1), 161–168.
Darzynkiewicz, Z., et al., 1997. Cytometry in cell necrobiology: analysis of apoptosis and accidental cell death (necrosis). Cytometry 27 (1), 1–20.
Davis, J.M., et al., 1991. Variations in the carcinogenicity of tremolite dust samples of differing morphology. Ann. N. Y. Acad. Sci. 643, 473–490.
De Matteis, S., et al., 2017. Current and new challenges in occupational lung diseases. Eur. Respir. Rev. 26 (146).
Degrandi, D., et al., 2009. The proinflammatory cytokine-induced IRG1 protein associates with mitochondria. J. Interf. Cytokine Res. 29 (1), 55–67.
Deville, S., et al., 2020. Time-resolved characterization of the mechanisms of toxicity induced by silica and amino-modified polystyrene on alveolar-like macrophages. Arch. Toxicol. 94 (1), 173–186.
Dikensoy, O., 2008. Mesothelioma due to environmental exposure to erionite in Turkey. Curr. Opin. Pulm. Med. 14 (4), 322–325.
Divangahi, M., King, I.L., Pernet, E., 2015. Alveolar macrophages and type I IFN in airway homeostasis and immunity. Trends Immunol. 36 (5), 307–314.
Dodson, R.F., Atkinson, M.A.L., Levin, J.L., 2003. Asbestos fiber length as related to potential pathogenicity: A critical review, 44(3), pp. 291–297.
Driscoll, K.E., et al., 1995. Alveolar macrophage cytokine and growth factor production in a rat model of crocidolite-induced pulmonary inflammation and fibrosis. J. Toxicol. Environ. Health 46 (2), 155–169.
Duncan, K.E., et al., 2014. In vitro determinants of asbestos fiber toxicity: effect on the relative toxicity of Libby amphibole in primary human airway epithelial cells. Part Fibre Toxicol 11, 2.
Dunning, K.K., et al., 2012. Mesothelioma associated with commercial use of vermiculite containing Libby amphibole. J. Occup. Environ. Med. 54 (11), 1359–1363.
Egilman, D., et al., 2019. Health Effects of Censored Elongated Mineral Particles: A Critical Review. Detection Limits in Air Quality and Environmental Measurements. ASTM International, West Conshohocken, PA, pp. 239–2019.
Fejer, G., et al., 2013. Nontransformed, GM-CSF-dependent macrophage lines are a unique model to study tissue macrophage functions. Proc. Natl. Acad. Sci. U. S. A. 110 (24), E2191–E2198.
Fensterl, V., Sen, G.C., 2015. Interferon-induced Ifit proteins: their role in viral pathogenesis. J. Virol. 89 (5), 2462–2468.

Garabrant, D.H., Pastula, S.T., 2018. A comparison of asbestos fiber potency and elongate mineral particle (EMP) potency for mesothelioma in humans. Toxicol. Appl. Pharmacol. 361, 127–136.
Geist, L.J., et al., 2000. Asbestos stimulation triggers differential cytokine release from human monocytes and alveolar macrophages. Exp. Lung Res. 26 (1), 41–56.
Ghio, A.J., et al., 2008. Iron homeostasis in the lung following asbestos exposure. Antioxid. Redox Signal. 10 (2), 371–377.
Giordano, G., et al., 2010. Type I interferon signaling contributes to chronic inflammation in a murine model of silicosis. Toxicol. Sci. 116 (2), 682–692.
Goodglick, L.A., Kane, A.B., 1990. Cytotoxicity of long and short crocidolite asbestos fibers in vitro and in vivo. Cancer Res. 50 (16), 5153–5163.
Group, E.R., 2003. Report on the Expert Panel on Health Effects of Asbestos and Synthetic Vitreous Fibers: The Influence of Fiber Length, 02421, p. 229. Lexington, MA.
Hamilton, R.F., Iyer, L.L., Holian, A., 1996. Asbestos induces apoptosis in human alveolar macrophages. Am. J. Phys. 271 (5 Pt 1), L813–L819.
Holian, A., et al., 1997. Asbestos and silica-induced changes in human alveolar macrophage phenotype. Environ. Health Perspect. 105 (Suppl. 5), 1139–1142.
Holt, P.G., 1986. Down-regulation of immune responses in the lower respiratory tract: the role of alveolar macrophages. Clin. Exp. Immunol. 63 (2), 261–270.
IARC, 2012. A Review of Human Carcinogens. Part C: Arsenic, metals, fibres, and dusts. International Agency for Research on Cancer.
IARC, 2017. IARC Working Group on the Evaluation of Carcinogenic Risks to Humans. Some Nanomaterials and Some Fibres. International Agency for Research on Cancer.
Ishida, T., et al., 2019. Live-cell imaging of macrophage phagocytosis of asbestos fibers under fluorescence microscopy. Genes Environ 41, 14.
Joshi, N., Walter, J.M., Misharin, A.V., 2018. Alveolar macrophages. Cell. Immunol. 330, 86–90.
Joshi, N., et al., 2020. A spatially restricted fibrotic niche in pulmonary fibrosis is sustained by M-CSF/M-CSFR signalling in monocyte-derived alveolar macrophages. Eur. Respir. J. 55 (1).
Kamp, D.W., Weitzman, S.A., 1999. The molecular basis of asbestos induced lung injury. Thorax 54 (7), 638–652.
Kohyama, N., et al., 2017. Lung cancer in a patient with predominantly short tremolite fibers in his lung. Am. J. Ind. Med. 60 (9), 831–838.
Laskin, D.L., Malaviya, R., Laskin, J.D., 2015. In: Parent, R.A. (Ed.), Pulmonary macrophages, in Comparative biology of the normal lung. Elsevier/AP, Academic Press is an imprint of Elsevier, Amsterdam; Boston, pp. 629–649.
Levresse, V., et al., 2000. DNA breakage in asbestos-treated normal and transformed (TSV40) rat pleural mesothelial cells. Mutagenesis 15 (3), 239–244.
Lippmann, M., 1988. Asbestos exposure indices. Environ. Res. 46 (1), 86–106.
Lippmann, M., 1990a. Effects of Fiber characteristics on lung deposition, retention, and disease. Environ. Health Perspect. 88, 311–317.
Lippmann, M., 1990b. Man-made mineral fibers (MMMF): human exposures and health risk assessment. Toxicol. Ind. Health 6 (2), 225–246.
Lippmann, M., 2014. Toxicological and epidemiological studies on effects of airborne fibers: coherence and public [corrected] health implications. Crit. Rev. Toxicol. 44 (8), 643–695.
Lippmann, M., Timbrell, V., 1990. Particle loading in the human lung—human experience and implications for exposure limits. J. Aerosol Med. 3 (s1) p. S-155-S-168.
Lowers, H., Meeker, G., Survey, G., 2002. Tabulation of asbestos-related terminology [electronic resource]. U.S. Department of the Interior, U.S. Geological.
Mandel, J.H., Alexander, B.H., Ramachandran, G., 2016. A review of mortality associated with elongate mineral particle (EMP) exposure in occupational epidemiology studies of gold, talc, and taconite mining. Am. J. Ind. Med. 59 (12), 1047–1060.
Manning, C.B., Vallyathan, V., Mossman, B.T., 2002. Diseases caused by asbestos: mechanisms of injury and disease development. Int. Immunopharmacol. 2 (2–3), 191–200.
Marczynski, B., et al., 1994. Increased incidence of DNA double-strand breaks and anti-ds DNA antibodies in blood of workers occupationally exposed to asbestos. Hum. Exp. Toxicol. 13 (1), 3–9.
Metcalf, R.V., Buck, B.J., 2015. Genesis and health risk implications of an unusual occurrence of fibrous NaFe3+−amphibole. Geology 43 (1), 63–66.
Metsalu, T., Vilo, J., 2015. ClustVis: a web tool for visualizing clustering of multivariate data using principal component analysis and heatmap. Nucleic Acids Res. 43 (W1). W566-70.
Middendorf, P., et al., 2011. Current intelligence bulletin 62: asbestos fibers and other elongate mineral particles: state of the science and roadmap for research. In: U.S. Department of Health and Human Services, Public Health Service, Centers for Disease Control and Prevention. National Institute for Occupational Safety and Health, DHHS (NIOSH) Cincinnati, OH, p. 173.
Miller, A., 2014. "Not your grandfather's pleural disease": rapid progression, ventilatory impairment, and chronic pleuritic pain from Libby vermiculite/amphibole. Am. J. Ind. Med. 57 (11), 1195–1196.
Miserocchi, G., et al., 2008. Translocation pathways for inhaled asbestos fibers. Environ. Health 7, 4.
Mossman, B.T., 2008. Assessment of the pathogenic potential of asbestiform vs. nonasbestiform particulates (cleavage fragments) in in vitro (cell or organ culture) models and bioassays. Regul. Toxicol. Pharmacol. 52 (1 Suppl), S200–S203.
Mossman, B.T., et al., 2011. Pulmonary endpoints (lung carcinomas and asbestosis) following inhalation exposure to asbestos. J Toxicol Environ Health B Crit Rev 14 (1–4), 76–121.
Moyer, V.D., et al., 1994. Oxygen radicals and asbestos carcinogenesis. Environ. Health Perspect. 102 (Suppl. 10), 131–136.
Msiska, Z., et al., 2010. DNA double-strand breaks by asbestos, silica, and titanium dioxide: possible biomarker of carcinogenic potential? Am. J. Respir. Cell Mol. Biol. 43 (2), 210–219.
Nagatomo, H., et al., 2007. Change of heme oxygenase-1 expression in lung injury induced by chrysotile asbestos in vivo and in vitro. Inhal. Toxicol. 19 (4), 317–323.
National Toxicology, P., 1990. NTP Toxicology and carcinogenesis studies of Tremolite (CAS no. 14567-73-8) in F344/N rats (feed studies). Natl Toxicol Program Tech Rep Ser 277, 1–183.
Oberdorster, G., Graham, U., 2018. Predicting EMP hazard: lessons from studies with inhaled fibrous and non-fibrous nano- and micro-particles. Toxicol. Appl. Pharmacol. 361, 50–61.
Okayasu, R., et al., 1999. Asbestos and DNA double strand breaks. Cancer Res. 59 (2), 298–300.
Pacella, A., et al., 2012. Iron topochemistry and surface reactivity of amphibole asbestos: relations with in vitro toxicity. Anal. Bioanal. Chem. 402 (2), 871–881.
Padmore, T., et al., 2017. Quantitative analysis of the role of fiber length on phagocytosis and inflammatory response by alveolar macrophages. Biochim. Biophys. Acta Gen. Subj. 1861 (2), 58–67.
Palekar, L.D., Spooner, C.M., Coffin, D.L., 1979. Influence of crystallization habit of minerals on in vitro cytotoxicity. Ann. N. Y. Acad. Sci. 330, 673–686.
Perkins, R.C., et al., 1993. Human alveolar macrophage cytokine release in response to in vitro and in vivo asbestos exposure. Exp. Lung Res. 19 (1), 55–65.
Pfau, J.C., et al., 2017. Comparative health effects in mice of Libby amphibole asbestos and a fibrous amphibole from Arizona. Toxicol. Appl. Pharmacol. 334, 24–34.
Pira, E., et al., 2017. Mortality of talc miners and millers from Val Chisone, northern Italy: an updated cohort study. J. Occup. Environ. Med. 59 (7), 659–664.
Roggli, V.L., 2018. Measuring EMPs in the lung what can be measured in the lung: asbestiform minerals and cleavage fragments. Toxicol. Appl. Pharmacol. 361, 14–17.
Schiller, J.E., Payne, S.L., Khalafalla, S.E., 1980. Surface charge heterogeneity in amphibole cleavage fragments and asbestos fibers. Science 209 (4464), 1530–1532.
Schneider, A., et al., 2019. Growth hormone-mediated reprogramming of macrophage transcriptome and effector functions. Sci. Rep. 9 (1), 19348.
Schraufnagel, D.E., Society, A.T., 2010. Breathing in America: Diseases, Progress, and Hope. American Thoracic Society.
Spencer, D.M., Gauley, J., Pisetsky, D.S., 2014. The properties of microparticles from RAW 264.7 macrophage cells undergoing in vitro activation or apoptosis. Innate Immun. 20 (3), 239–248.
Stichling, N., et al., 2018. Lung macrophage scavenger receptor SR-A6 (MARCO) is an adenovirus type-specific virus entry receptor. PLoS Pathog. 14 (3), e1006914.
Suo, S., et al., 2018. Revealing the critical regulators of cell identity in the mouse cell atlas. Cell Rep. 25 (6), 1436–1445 (e3).
Vincenten, J., et al., 2017. Barriers and Facilitators to the Elimination of Asbestos Related Diseases-Stakeholders' Perspectives. Int. J. Environ. Res. Public Health 14 (10).
Weill, D., 2018. Proceedings of the Monticello conference on elongate mineral particles (EMP). Toxicol. Appl. Pharmacol. 361, 1–2.
Wlodkowic, D., Skommer, J., Darzynkiewicz, Z., 2010. Cytometry in cell necrobiology revisited. Recent advances and new vistas. Cytometry A 77 (7), 591–606.
Woo, M., et al., 2018. Mycobacterium tuberculosis infection and innate responses in a new model of lung alveolar macrophages. Front. Immunol. 9, 438.
World Health, O., 2000. Air quality guidelines for Europe. In: WHO Reg Publ Eur Ser, 91 p. V-X, 1–273.
Yanamala, N., et al., 2018. Characterization of pulmonary responses in mice to asbestos/asbestiform fibers using gene expression profiles. J Toxicol. Environ. Health A 81 (4), 60–79.
Yang, H.Y., Shie, R.H., Chen, P.C., 2013a. Pulmonary fibrosis in workers exposed to non-asbestiform tremolite asbestos minerals. Epidemiology 24 (1), 143–149.
Yang, H.Y., Shie, R.H., Chen, P.C., 2013b. Carving of non-asbestiform tremolite and the risk of lung cancer: a follow-up mortality study in a historical nephrite processing cohort. Occup. Environ. Med. 70 (12), 852–857.
Yang, H., et al., 2017. The haptoglobin beta subunit sequesters HMGB1 toxicity in sterile and infectious inflammation. J. Intern. Med. 282 (1), 76–93.